DISCRETE THERMODYNAMICAL MODELLING OF TRAFFIC STREAMS

Milan Krbálek, Faculty of Nuclear Sciences and Physical Engineering, Czech Technical University of Prague, Trojanova 13, Prague, 12000, Czech Republic

ABSTRACT

We present some important results of a robust statistical analysis applied to freeway traffic data measured by induction double-loop detectors. We demonstrate that the microscopic quantities of traffic flow (e.g. clearance distribution, mental strain coefficient, spectral rigidity and so on) markedly depend on an actual position of the traffic sample in the fundamental diagram (traffic flux vs. traffic density). Furthermore, we show that clearance distribution and spectral rigidity of the celebrated Nagel-Schreckenberg model (NaSch-model) do not correspond to realistic traffic behaviour, although such a model reproduces most of macroscopic traffic phenomena accurately. Exploiting new knowledge on local thermodynamical features of vehicular streams we introduce thermal-like variant of the cellular NaSch-model, which is powerful in both microscopic and macroscopic analysis of traffic.

Keywords: Traffic Modelling, Microscopic Structure of Traffic, Random Matrix Theory

STATISTICAL ANALYSIS OF MICROSCOPIC STRUCTURE OF TRAFFIC SAMPLE

Currently, the traffic researches put the stronger accent on microscopic structure of traffic. Besides the macroscopic quantities (traffic flux J and traffic density ρ) the scientific literature on traffic introduces the following microscopic description. Considering the data samples $\{t_1, t_2, \dots, t_N\}$, $\{t'_1, t'_2, \dots, t'_N\}$ of times when the ith car has entered, resp. left the induction loop detector, and the samples $\{v_1, v_2, \dots, v_N\}$ of car's velocities one can calculate the distance clearance (for ℓth car) as

$$r_\ell = (t'_{\ell-1} - t_\ell)\, v_\ell.$$

It represents a bumper-to-bumper distance, i.e. clear distance between subsequent vehicles in the traffic stream. We remark that the calculated clearance comprises the estimation only because of possible acceleration/deceleration of vehicles. Evidently, such a quantity has statistical nature and it is therefore appropriate to specify it with the help of statistical approaches. For this purpose we use the scaled probability density $\wp(r)$ for distance clearance (clearance distribution) fulfilling the standard proper normalisation

$$\int_{\mathbb{R}} \wp(r)\,\mathrm{d}r = 1$$

and the scaling condition

$$\langle r \rangle = \int_{\mathbb{R}} r\,\wp(r)\,\mathrm{d}r = 1.$$

The latter assures the mean clearance among the following vehicles is re-scaled to one. Processing a huge amount of data (see Figure 1) we confirm the general knowledge on fundamental diagram $J = J(\rho)$. Such a dependence shows the significant hysteretic features reflecting the crowding effects usually observed in realistic transport systems (e.g. congested states, stop-and-go states). Whereas the main part (for densities up to 40 vehicles/lane/km) of the fundamental diagram corresponds to the free flow states (mean velocity is above 100 km/hour) the right-hand side of the diagram displays the congested traffic states where the freeway is extensively saturated. It leads to a rapid descent in the mean velocity of cars, which is predominantly caused by concerns of drivers about the possible collision with the other vehicles. Intermediate interval of densities (between 40 and 50 vehicles/lane/km) is the region of metastable traffic states, where the vehicular samples convert from free to congested area and vice versa.

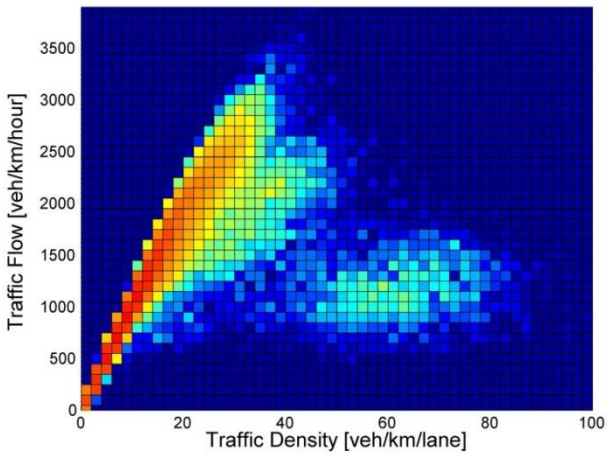

Figure 1 – Colour Representation of Fundamental Diagram. The complete data record (containing single-vehicle data measured in 60 days in three-lane freeway) has been divided into samples of one hundred succeeding cars. For each sample the flux and density has been calculated. The shades of colours are proportional to the number of those samples belonging to the corresponding region of fundamental diagram.

Clearance Distribution in Traffic Samples

As published in previous articles [Krbalek and Helbing 2004, Helbing et al. 2006, Krbalek 2007, Krbalek 2008] a suitable candidate for distance clearance distribution is a one-parametric class of functions

$$\wp_\beta(r) = \Theta(r)\,\mathrm{A}\exp\left[-\frac{\beta}{r} - Br\right],$$

where the only free parameter β is the inverse thermodynamical temperature (see [Sopasakis 2004]). Actually, the hypothesis about the psychological interpretation of β is being verified. Within the bounds of the upcoming research project the thermal parameter β is interpreted as a psychological coefficient describing a level of the mental pressure under the driver is while driving his/her car. Hence, in the next part of this article we call β as a mental strain coefficient. We remark that the symbol

$$\Theta(r) = \begin{cases} 1 \ldots r \geq 0, \\ 0 \ldots r < 0, \end{cases}$$

denotes the Heaviside's function and two normalization constants can be calculated [see Krbalek 2007] via two formulas

$$B = \beta + \frac{3 - \exp\left[-\sqrt{\beta}\right]}{2},$$

$$A^{-1} = 2\sqrt{\frac{\beta}{B}}\,\mathrm{K}_1\left(2\sqrt{B\beta}\right).$$

Here $\mathrm{K}_\lambda(x)$ represents the modified Bessel's function of the second kind (so-called MacDonald's function) of the λ-th order. For clearness, below we plot the clearance distribution obtained from traffic data measured on a signal-controlled crossroad during the time interval when vehicles were waiting for a green signal.

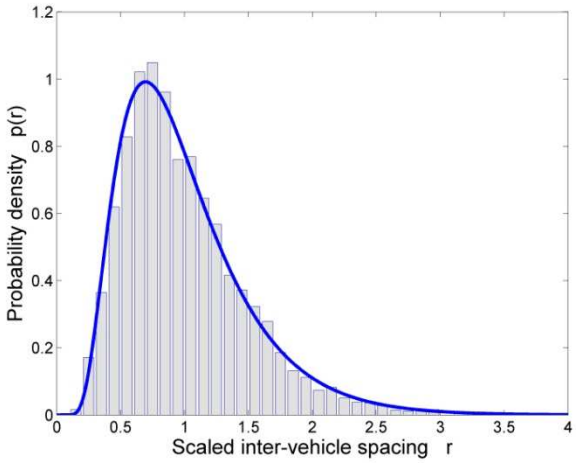

Figure 2 – Clearance Distribution of Cars Waiting at the Red Signal on a Signal-Controlled Crossroad. Bars correspond to the crossroad data and the curve displays the predicted probability density $\wp_\beta(r)$ where the mental strain coefficient is estimated at the value $\beta \approx 1.45$. We note that the single-vehicle data were analysed separately for different lanes of the two-lane road.

The measured distances are successfully compared to the probability density $\wp_\beta(r)$ cited above. In fact, the inter-vehicle gap distribution is rapidly changing with the location of the traffic sample in the fundamental diagram. Especially, in the region of the congested states the small change in flux or density substantially affects the gap distribution observed, which is so typical for classical or quantum chaotic systems. For more comprehensible understanding of how the clearance distribution is depending on flux J and density ρ, we execute the robust statistical analysis of highway data (three-lane unidirectional freeway, no on-ramps, no off-ramps) with the following results. In the region of free-flow states one can observe the exponential probability density (approximately), which is expected for ensembles

of statistically independent events or elements. In this case the mental strain coefficient is very low and therefore the corresponding distribution converges to the limiting state

$$\lim_{\beta\to 0} \wp_\beta(r) = \lim_{\beta\to 0} \Theta(r)\, \mathrm{A} \exp\left[-\frac{\beta}{r} - Br\right] = \Theta(r)\exp[-r].$$

With the growing density (as the driver's psychological pressure increases) the inter-vehicle gap distribution shows stronger repulsion near the origin, which is evident when calculating the limit

$$\lim_{r\to 0_+} \wp_\beta(r) = \lim_{r\to 0_+} \frac{\wp_\beta(r)}{r^n} = 0 \ (\mathrm{n} \in \mathbb{N}, \beta > 0).$$

Such an effect finally leads to the instability of free flow and consecutively to the transition into the new traffic state – the congested flow.

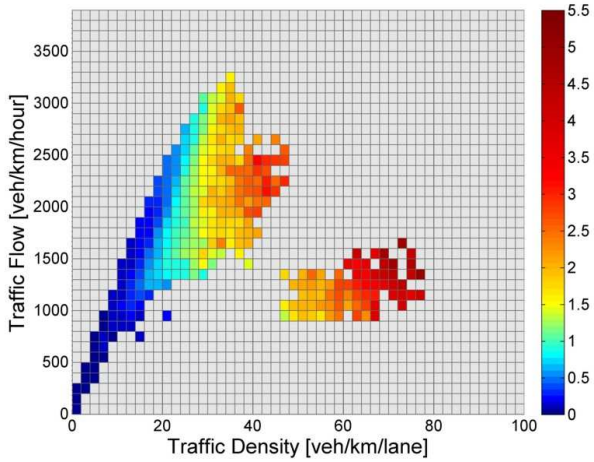

Figure 3 – Colour Visualization of Mental Strain Coefficient for Car Drivers. The colour scale (see legend on right-hand side) displays the value of parameter β depending on both the traffic flux and density. Notice the local decrease in the strain coefficient around 40 veh/km/lane. The similar decrease has been detected in other data as well.

As visible in Figure 3 the dependence $\beta = \beta(\varrho, J)$ of the strain coefficient on the traffic flux and density shows a meaningful (and predictable) behaviour. Whereas in the region of low densities one can observe the insignificant level of strain, with the growing density the parameter β is increasing. It finally culminates in the region of metastability

$$(\rho, J) \in (30{,}50) \times (1800{,}2500).$$

The strong level of psychological pressure (under which the driver is if moving in this region) causes the saturation of free-flow phase, which results in the change of traffic phase. After the transition into the congested-flow phase the driver's strain is temporarily decreasing, which is influenced by the sharp drop of mean velocity. Owing to the lower speed of car the driver's ability to operate the vehicle is markedly better than in the region of metastability. However, if the traffic density is further increasing the psychological pressure is noticeably accretive again. The growth of parameter β to the critical boundary (around $\beta_{\mathrm{crit}} \approx 4$) leads to the creation of the self-organized blocs of vehicles moving in stop-and-go waves. As demonstrated the inverse temperature serves as a convenient indicator for stability/instability of actual traffic state. Thus, the hypothesis on psychological interpretation of β appears to be legitimate.

Spectral Rigidity of Traffic Stream

Another way how to inspect the microscopic structure of vehicular ensembles is to investigate a so-called spectral rigidity of traffic sample. Such a statistical quantity is not usual in the physics of traffic, however, the related quantity was already introduced by Helbing et al in the article [Helbing 2003]. For the first time the spectral rigidity of traffic streams was elaborately studied in article [Krbálek and Šeba 2009].

Contrary to the clearance distribution the spectral rigidity $\Delta(L)$ describes the statistical properties in the extensive clusters of neighbouring cars. Concretely, let $\{r_\ell : \ell = 1, \dots, N\}$ be the set of scaled clearances measured between each pair of subsequent cars moving in the same lane. Dividing the entire sample $[0, N)$ into subintervals

$$S_\ell^L := [(\ell - 1)\mathrm{L}, \ell\mathrm{L}), \quad \ell = 1, \dots, \lfloor N/L \rfloor$$

of a length L and denoting by $n_\ell(L)$ the number of vehicles inside the subinterval S_ℓ^L, the average value $\bar{n}(L)$ taken over all possible subintervals is

$$\bar{n}(L) = \frac{1}{\left\lfloor \frac{N}{L} \right\rfloor} \sum_{\ell=1}^{\left\lfloor \frac{N}{L} \right\rfloor} n_\ell(L),$$

where the integer part $\lfloor N/L \rfloor$ stands for the number of all subintervals S_ℓ^L included in the interval $[0, N)$. Because of the scaling $\langle r \rangle = 1$ it holds $\bar{n}(L) = L$.

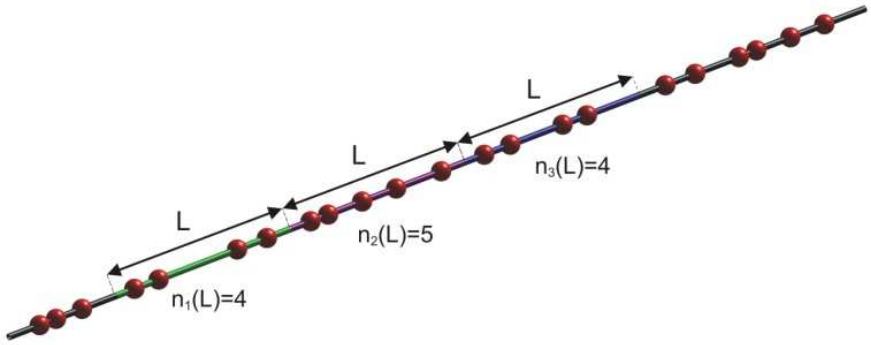

Figure 4 – Illustrating the Spectral Rigidity Analysis.

The spectral rigidity $\Delta(L)$ is a function of the length L and is defined as variance

$$\Delta(L) = \frac{1}{\lfloor N/L \rfloor} \sum_{\ell=1}^{\left\lfloor \frac{N}{L} \right\rfloor} (n_\ell(L) - L)^2.$$

In fact, this formula represents the statistical variance of the number of vehicles moving at the same time inside a fixed part of the road of a length L.

The mathematical properties of the $\Delta(L)$ are well understood owing to the fact that they have been elaborately studied under terms of Random Matrix Theory. As well known, the behaviour of the spectral rigidity reflects the level of systemization in the ensemble. If the system is random completely (i.e. without any regulation) the rigidity is equal to identity, i.e.

$\Delta(L) = L$. On the contrary, any mutual interactions among the elements of ensemble cause a descent in the slope χ of a curve $\Delta(L) \approx \chi L + \gamma$ ($\chi < 1$). Finally, if the ensemble is organized perfectly (i.e. all neighbouring particles have the same spacings), the relevant rigidity is zero.

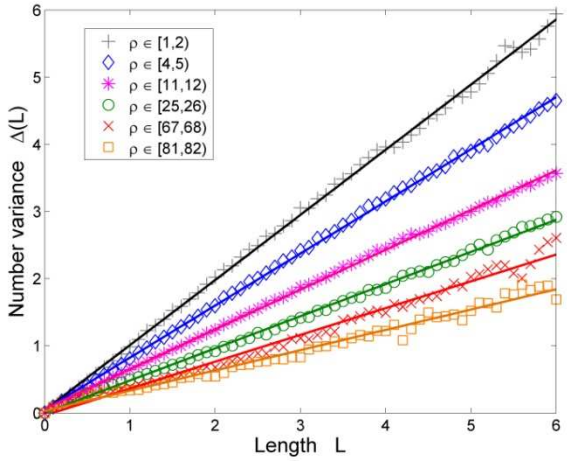

Figure 5 – Spectral Rigidity Test of Traffic Flow. Plus signs, diamonds, stars, circles, crosses and squares represent the spectral rigidity of the real-road data. We plot the 60-days averages calculated for data from the quoted density regions (see legend). For details see [Krbálek and Šeba 2009]. The curves show the linear approximations of the individual data.

The recent investigations (published in [Krbálek and Šeba 2009]) has revealed that the spectral rigidity investigated for induction-double-loop-detector data is a linear function of length L in all density regimes, i.e.

$$\Delta(L) = \chi L + \gamma + o(L^{-1}),$$

where $\chi = \chi(\varrho)$ and $\gamma = \gamma(\varrho)$. Moreover, the detailed statistical analysis of traffic data has ascertained that the rigidity depends not only on density but on flux as well. The result of relevant statistical investigations is visualized in the Figure 6.

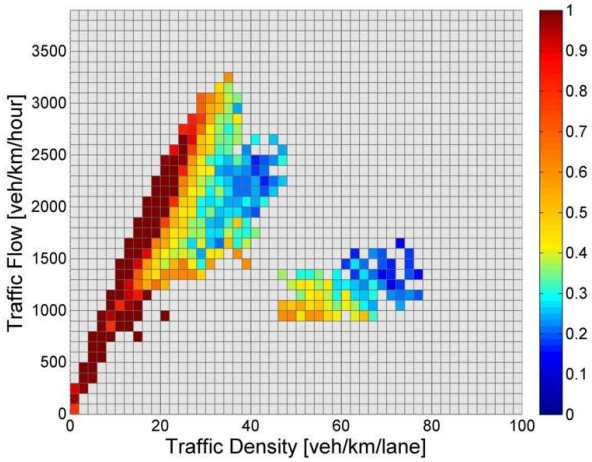

Figure 6 – Colour Visualization of Spectral Rigidity. The colour scale (see legend on right-hand side) displays the slope $\chi = \chi(\varrho, J)$ (depending on traffic density and flux) in the linear behaviour of spectral rigidity $\Delta(L)$.

MICROSCOPIC ANALYSIS OF CELLULAR TRAFFIC MODEL

One of the most famous (and frequently used) traffic model is the cellular model originally developed by Kai Nagel and Michael Schreckenberg (see [Nagel and Schreckenberg 1992]). Although during the last twenty years many alternatives of NaSch-model has been created (e.g. [Rickert et al. 1996], [Fukui and Ishibashi 1996], [Nishimura et al. 2006]), in fact all essential properties concerning this article are independent of the variant of the model. Therefore we are focused on the original arrangement of the model.

Consider n particles located in the chain of N sites and define the particle density by the simple formula $\varrho = \frac{n}{N}$. Let $v_{max} \in \mathbb{N}$ be the maximal permissible velocity of model's particles. Due to the condition that each cell of the chain is either occupied or empty, any allowable configuration of the model is therefore unequivocally described by the sets of the ordered particle locations $\{x_\ell \in \mathbb{N} : \ell = 1, \dots, n\}$ and particle velocities $\{v_\ell \in \hat{v}_{max} : \ell = 1, \dots, n\}$. We note that symbol $\hat{v}_{max}$ represents the set $\{1,2,3, \dots, v_{max}\}$. Denoting $p \in [0,1]$ the randomisation parameter, we introduce the basic scheme of the NaSch-model in the following steps.

- Step 1 (Startup): The timer is set for zero, i.e. $t = 0$. The starting configuration $(x_1(t), x_2(t), \dots, x_n(t))$ and $(v_1(t), v_2(t), \dots, v_n(t))$ is chosen randomly with respect to the above-mentioned restrictions.
- Step 2 (Updating the Configuration): The previous configuration is understood as an initial one. The timer is shifted by one, i.e. $t \equiv t + 1$.
- Step 2 (Distance Evaluation): The distances $r_\ell(t) = x_{\ell+1}(t) - x_\ell(t)$ among the successive particles are calculated.
- Step 3 (Acceleration): If the car velocity is less than maximal velocity the car accelerates according the rule $v_\ell(t + \frac{1}{3}) = v_\ell(t) + 1$.
- Step 4 (Randomization): The velocities of all particles are randomly reduced by one, i.e. $v_\ell(t + \frac{2}{3}) = v_\ell(t + \frac{1}{3}) - 1$ with probability p (uniformly distributed).
- Step 5 (Averting the Collision): If $v_\ell(t + \frac{2}{3}) > r_\ell(t)$ the car velocity is reduced to avoid the possible collision, i.e. $v_\ell(t + 1) = r_\ell(t) - 1$, otherwise the velocity remains unchanged, i.e. $v_\ell(t + 1) = v_\ell\left(t + \frac{2}{3}\right)$.
- Step 6 (Parallel Motion): New particles positions are obtained applying the rule $x_\ell(t + 1) = x_\ell(t) + v_\ell(t + 1)$. All particles move at the same time (parallel updating).
- Step 7 (Return): The procedure described is multiplicatively repeated by returning to the Step 2.

Analysis of microscopic structure

Although it is well known that cellular traffic models – based on the above-mentioned principles – predict successfully the effects of crowding (traffic jams etc.) the local structure of such models is in deep inconsonance with the traffic reality. Evidently, this discrepancy is strongly undesirable because it brings out many problems in model interpretation. The

reasons for such a dissent can be predominantly found in the time discretisation and space discretization of the models. Anyway, the cellular character of the modelled particle-ensemble leads to particle interactions which are of a different origin than those detected in realistic flows.

In the following part of our text we demonstrate the above-mentioned inconsonance. For these intentions we have used the NaSch-model with the following fixed parameters: $v_{max} = 8$, $p = 0.5$ and $N = 10000$. The density ϱ was varied to obtain a more precise notion of changes in microstructure of relevant steady states. We have applied the densities: $\varrho \in \left\{\frac{25}{1000}, \frac{1}{10}, \frac{3}{10}, \frac{55}{100}\right\}$. The Figures 7, 8, 9, and 10 show how the corresponding clearance distributions of Nagel-Schreckenberg model are changing with density.

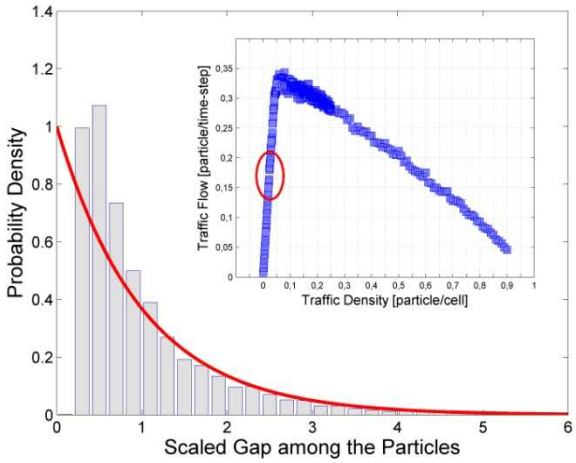

Figure 7 – Scaled Inter-Particle Gap Distribution for NaSch-Model. The histogram was obtained for value $\varrho = \frac{25}{1000}$. The clearances of cellular automata have been computed directly from relevant simulations, which is in small inconsonance with realistic measurements.

If the density of model is low (i.e. in the region of free flows) the inter-particle gap distribution shows practically exponential behaviour $\wp_\beta(r) = \Theta(r)\exp[-r]$. It corresponds to the fact that interactions among the free-flow-particles are negligible.

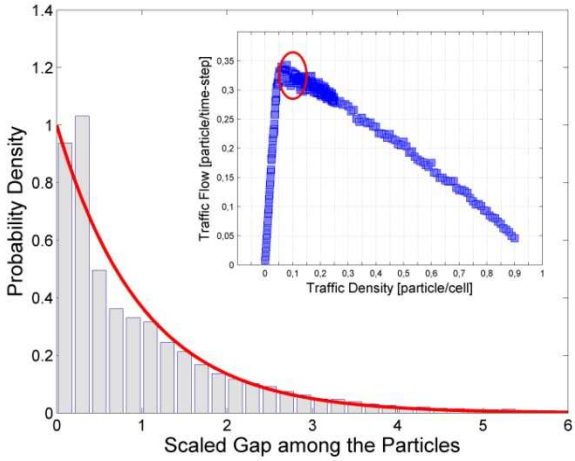

Figure 8 – Scaled Inter-Particle Gap Distribution for NaSch-Model. The histogram was obtained for value $\varrho = \frac{1}{10}$.

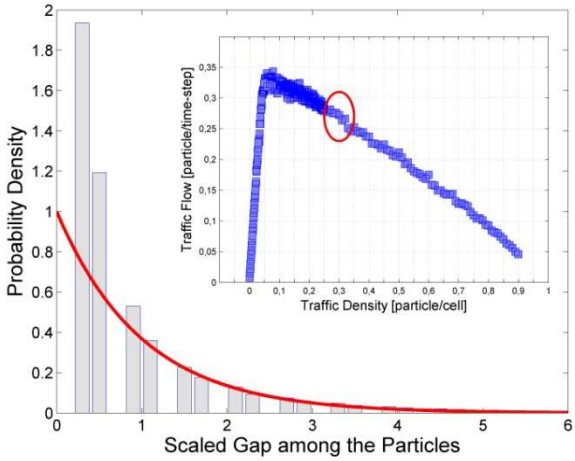

Figure 9 – Scaled Inter-Particle Gap Distribution for NaSch-Model. The histogram was obtained for value $\varrho = \frac{3}{10}$.

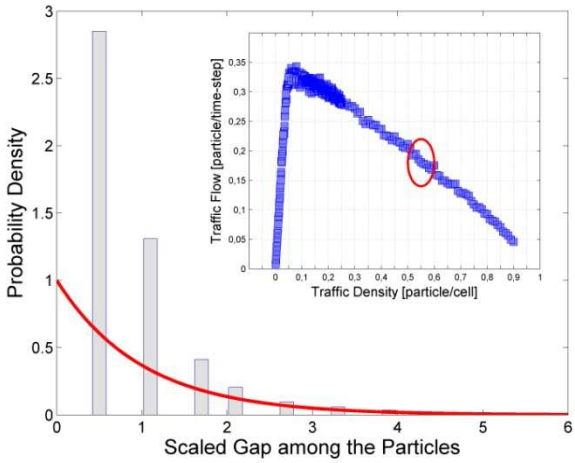

Figure 10 – Scaled Inter-Particle Gap Distribution for NaSch-Model. The histogram was obtained for value $\varrho = \frac{55}{100}$.

However, with the increasing density the scaled clearance distribution is passing into the behaviour that does not correspond to that revealed in freeway data. In the region of highly saturated states the particles create long queues (with small gaps among succeeding particles), which leads to the discontinuities in the graph $\wp = \wp(r)$ (being re-scaled according to the condition $\langle r \rangle = 1$). These difficultly-interpreted states could be detected also when investigating the spectral rigidity. Anyway, if the graph of spectral rigidity $\Delta = \Delta(L)$ is situated above the identity $\Delta(L) = L$, the model-setting produces incorrect steady states.

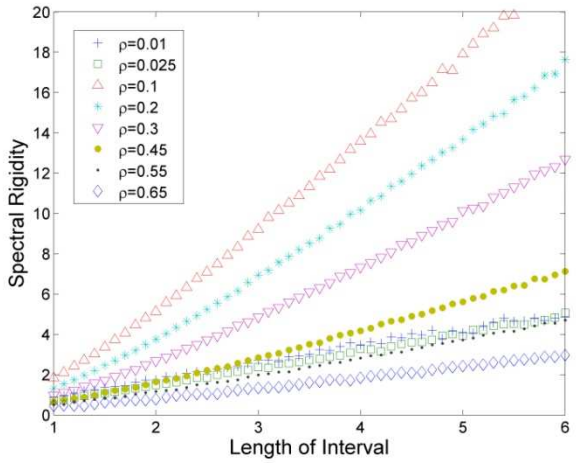

Figure 11 – Spectral Rigidity of Nagel-Schreckenberg Model. The parameters of the model have been fixed to $v_{max} = 8$, $p = 0.5$ and $N = 10000$. The model density is varied as indicated in the legend.

It will be shown later that the unwelcome effects detected by the above-mentioned statistical analysis can be eliminated if implementing a thermal approach (on local scale).

THERMAL-LIKE CELLULAR MODEL OF TRAFFIC

It has been published many times [Krbalek and Helbing 2004], [Sopasakis 2004], [Mahnke et al. 2007], [Krbalek and Šeba 2009] that some of driven systems (including the traffic systems) show certain features corresponding to those detected in the thermal systems, i.e. in systems tending towards the thermal equilibrium. Traffic samples, however, shows such a behaviour on local scale only. Thus the thermal approach to the traffic modelling may not be applied completely but partially only.

Globally, two alternative methods of traffic modelling used to be applied. Whereas the cellular traffic models (as models operating in discrete areas or in discrete time) give a true picture of macroscopic effects of vehicular ensembles (traffic congestions and the like), the thermodynamical approaches (using the potential energy description) provide the correct picture of microscopic structure of traffic streams. Concurrently, a lot of thermodynamical models has been represented by the relevant numerical schemes. Some of them have been successfully used when simulating the real road traffic. For example, in the article [Krbalek 2008] the original alternative of Metropolis algorithm has plausibly reproduced the move of a vehicle sample in the vicinity of signal-controlled crossroads. Implementing such a new

familiarity to the surviving cellular traffic models we introduce a new variant of one-dimensional lattice gas which is powerful in both microscopic and macroscopic analysis of traffic.

The model parameters and initial state

Consider n particles randomly located on the circular lattice of length n that contains N cells. The particle density (and a length of one cell) is therefore equal to $\varrho = \frac{n}{N}$. Let $w \in \mathbb{N}$ be the maximal permissible length (number of cells) of the particle jump. Let the ordered positions $\{x_\ell \in \mathbb{N}: \ell = 1, \dots, n\}$ constitute the initial state for our simulation. Owing to the previous definitions the mean distance between two successive particles is equal to one, i.e.

$$\sum_{\ell=1}^{n} r_\ell = n,$$

where $r_\ell = (x_{\ell+1} - x_\ell)\varrho$ represents the real gap between $(\ell+1)$th and ℓth particles.

Since introducing the thermal variant of the cellular traffic model we define the potential quasi-energy of the actual configuration as

$$U = U(s_1, s_2, \dots, s_n) = \sum_{\ell=1}^{n} \frac{1}{s_\ell}, \qquad (1)$$

where $s_\ell = m\left\lceil \frac{r_\ell}{m} \right\rceil$ is the discretized distance among the particles. We note that the brackets $\lceil\ \rceil$ represent the upper integer part of the real number and the parameter $m \in (n, N]$ quantifies the intensity of discretization. We remark that the power-law potential in the previous formula is chosen with the respect to results published in [Krbalek and Helbing 2004] and confirmed in [Krbalek 2007, Krbalek and Šeba 2009]. Finally, the inverse termodynamical temperature is considered (for purposes of this article) to be proportional to the particle density, i.e. $\beta_{model} \sim \varrho$ (see [Sopasakis 2004]).

The model scheme

The particle positions are repeatedly updated (we use 20000 steps in our version) according to the following rules:

Step 1: The potential energy U_0 (using formula (1)) for the actual set of locations $(x_1, x_2, \dots, x_n)$ is calculated.
Step 2: We pick an index $\ell \in \{1,2, \dots, n\}$ at random.
Step 3: We draw a random number δ equally distributed in the interval $(0,1)$.
Step 4: The anticipated length of jump is discretized according to the formula $\tilde{w} = \lceil w\delta \rceil$.
Step 5: We compute an anticipated position $x'_\ell = x_\ell + \tilde{w}$ of the ℓth element. Because of singularity in the potential energy (1) the model particles can not change their order. Therefore we accept x'_ℓ only if $x'_\ell < x_{\ell-1}$.
Step 6: We calculate a value of potential energy U' determined for configuration $(x_1, x_2, \dots, x_{\ell-1}, x'_\ell, x_\ell, \dots, x_n)$.

Step 7: If $U' < U_0$ the ℓth particle position take on a new value x'_ℓ. If $U' \geq U_0$ then the Boltzmann factor

$$q = \exp\left[-\beta_{model}(U' - U_0)\right]$$

should be compared with a random number g equally distributed in $(0,1)$. Provided that the inequality $q > g$ is fulfilled the ℓth particle position takes on the new value x'_ℓ too. Otherwise, the original configuration $(x_1, x_2, \ldots, x_n)$ remains unchanged.

The outlined scheme of the updating procedure ensures a relaxation of ensemble into a equilibrium-like state when the quasi-energy fluctuates around a constant value being independent of initial configuration of particles. After reaching the balance (i.e. after approximately 5000 updates of configuration) the ensemble lingers in this steady state until the simulation is interrupted. We call this state as thermal quasi-equilibrium.

Macroscopic behaviour of the model

In spite of thermal nature of the model presented the macroscopic analysis uncovers the effects of aggregation leading to the congested traffic states. This is apparent when investigating the particle trajectories (see Figure below).

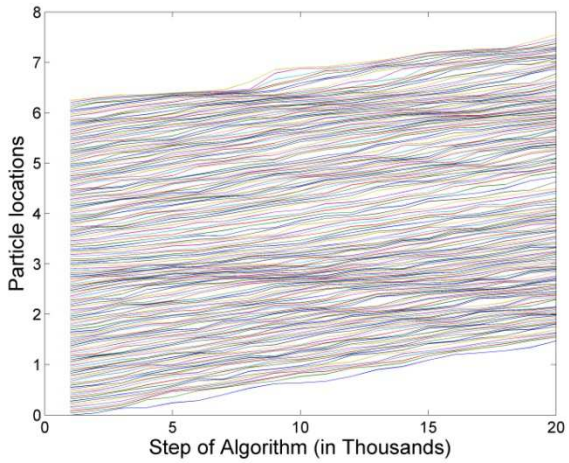

Figure 12 – Time Trajectories of the Thermal-like Cellular Model. In specific regions one can detect the local traffic congestions.

The phenomenon of traffic congestion can be detected also if analysing the fundamental diagram of the model. The detailed survey of the dependence $J = J(\varrho)$ shows that model generates the free flow states (in the region of small densities) as well as the saturated states (in the region of large densities). One representative of extensive family of fundamental diagrams is visualised in the Figure 13.

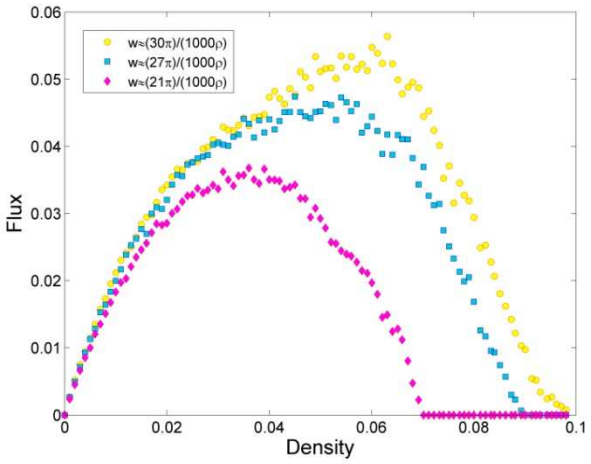

Figure 13 – Fundamental Diagram of Thermal-like Cellular Model. Data were obtained for $n = 200$, $\beta_{model} = 40\varrho$ and $m = 10$. The maximal jump-length has been varied as indicated in the legend.

Microscopic behaviour of the model

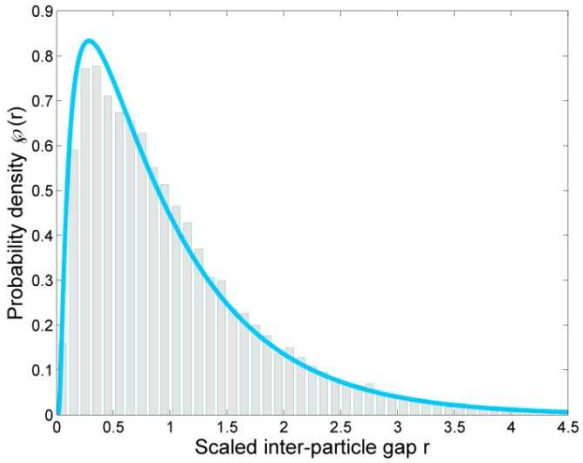

Figure 14 – Clearance Distribution Obtained for $\varrho = \frac{1}{400}$.

Due to the thermal background of the simulating scheme there is not surprising that the probability density for inter-particle distance shows (in all density regions) the behaviour expected. Anyway, considering the parameters $n = 200$, $\varrho \in \{\frac{1}{400}, \frac{1}{40}, \frac{1}{8}\}$ and $m = 10$, $w = \frac{3\pi}{100\varrho}$ and $\beta_{model} = 40\varrho$ we find out that the relevant clearance distributions obey the predictions obtained by the calculations (using the methods developed for Random Matrix theory) presented in the articles [Krbalek 2007], [Krbalek and Šeba 2009]. Concretely, the clearance distance distribution reads as

$$\wp_\beta(r) = \Theta(r)\, \mathrm{A} \exp\left[-\frac{\beta}{r} - Br\right],$$

where $\beta \approx \beta_{model}$.

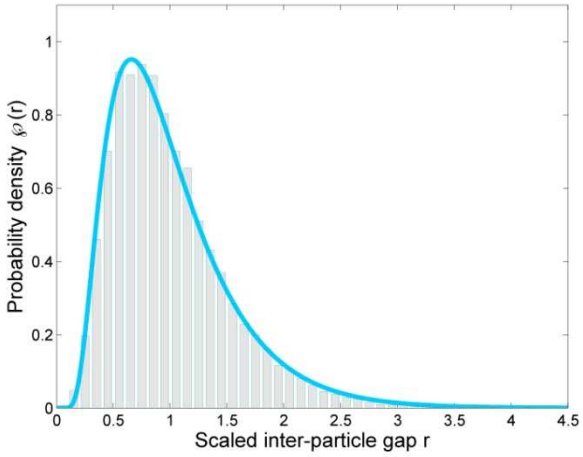

Figure 15 – Clearance Distribution Obtained for $\varrho = \frac{1}{40}$.

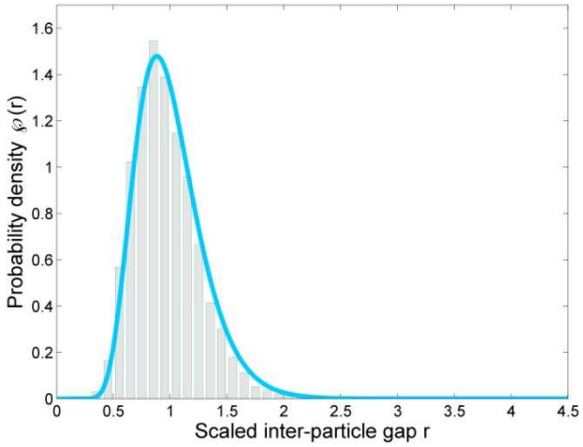

Figure 16 – Clearance Distribution Obtained for $\varrho = \frac{1}{8}$.

Similarly, the spectral rigidity of the model shows a linear behavior according the formula

$$\Delta(L) \approx \chi L + \gamma,$$

where

$$\chi(\beta) = \frac{2 + \sqrt{B\beta}}{2B(1 + \sqrt{B\beta})}, \quad \gamma(\beta) = \frac{6\sqrt{B\beta} + B\beta(21 + 4B\beta + 16\sqrt{B\beta})}{24(1 + \sqrt{B\beta})^4}.$$

The results of the respective analysis are pictured in the last Figure.

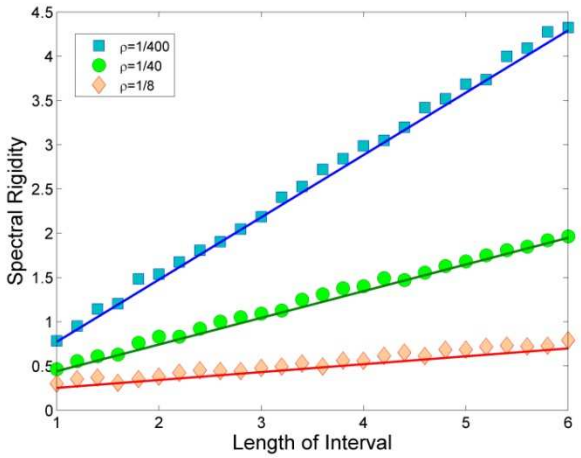

Figure 17 – Spectral Rigidity of the Thermal-like Cellular Model. The particle density has been varied as indicated in the legend.

SUMMARY AND CONCLUSION

We have introduced a new variant of one-dimensional lattice gas based on the principles known from thermodynamical systems. Connecting two different approaches (cellular and thermodynamical) we have created a new simulation scheme that produces the traffic model being in a deep accordance with the realistic traffic flow. Except the macroscopic effects (as phenomena of vehicle aggregation: congested states, traffic jams et al.) the above-mentioned thermal-like cellular automaton generates the steady states in such a way that the microscopic structure of the relevant ensembles shows the identical probability distributions as those revealed in data measured on various freeways.

Although there can be many objections against the thermal traffic models, the test of spectral rigidity (known from theory of quantum chaos and Random Matrix Theory) of the originated model clearly affirms that the local fluctuations of the thermal-model elements are of the same type as those detected among the real vehicles.

The presented idea to interconnect the discrete approach with the thermodynamical one is original and it is derived from the numerous attempts to apply the statistical physics principles to theory of traffic. On the other hand this article represents only a challenge in this field (similarly as published in [Sopasakis 2004]) and requires therefore many calibrations and improvements.

BIBLIOGRAPHY

Nagel, K. and M. Schreckenberg (1992). A cellular automaton model for freeway traffic. Journal de Physique I, France, 2, 2221.

Rickert, M. and K. Nagel and M. Schreckenberg and A. Latour (1996). Two lane traffic simulations using cellular automata. Physica A, 231(4), 534.

Fukui, M. and Y. Ishibashi (1996). Traffic flow in 1d cellular automaton model including cars moving with high speed. J. Phys. Soc. Jpn., 65, 1868

Neubert, L. and L. Santen and A. Schadschneider and M. Schreckenberg (1999). Single-vehicle data of highway traffic: A statistical analysis. Phys. Rev. E, 60**,** 6480

Chowdhury, D. and L. Santen and A Schadschneider (2000). Statistical physics of vehicular traffic and some related systems. Physics Reports 329, 199

Nishinari, K. and M. Treiber and D. Helbing (2003). Interpreting the wide scattering of synchronized traffic data by time gap statistics. Phys. Rev. E, 68, 067101

Krbálek, M. and D. Helbing (2004). Determination of interaction potentials in freeway traffic from steady-state statistics. Physica A, 333, 370

Sopasakis, A (2004). Stochastic noise approach to traffic flow modeling. Physica A, 342, 741

Knospe, W. and L. Santen and A. Schadschneider and M. Schreckenberg (2004). Phys. Rev. E, 70, 016115

Helbing, D. and M. Treiber and A. Kesting (2006). Understanding widely scattered traffic flows, the capacity drop, and platoons as effects of variance-driven time gaps. Physica A, 363, 62.

Nishimura, Y. and T. Cheon and P. Šeba (2006). Metastable congested states in multisegment traffic cellular automaton. J. Phys. Soc. Jpn., 75, 014801

Krbálek, M. (2007). Equilibrium distributions in thermodynamical traffic gas. J. Phys. A: Math. Theor., 40, 5813.

Mahnke R. and J. Kaupužs and J. Hinkel and H. Weber (2007). Application of thermodynamics to driven systems, Eur. Phys. J. B, 57, 463

Krbálek, M. (2008). Inter-vehicle gap statistics on signal-controlled crossroads. J. Phys. A: Math. Theor., 41, 205004

Alperovich, T. and A. Sopasakis (2008). Stochastic Description of Traffic Flow. Jour. Stat. Phys., 133, 1083

Appert-Rolland, C. (2009). Experimental study of short range interactions in vehicular traffic. Phys. Rev. E, 80, 036102

Krbálek, M. and P. Šeba (2009). Spectral rigidity of vehicular streams (Random Matrix Theory approach). J. Phys. A: Math. Theor., 42, 345001